J Mater Sci (2010) 45:5611–5623
DOI 10.1007/s10853-010-4626-x

The compression-after-impact strength of woven and non-crimp fabric reinforced composites subjected to long-term water immersion ageing

K. Berketis · D. Tzetzis

Received: 22 February 2010 / Accepted: 15 May 2010 / Published online: 9 June 2010

Abstract The current work examines the durability of composites reinforced with glass fibre woven fabric as well as non-crimp fabrics (NCF) immersed in water at 43, 65 and 93 °C for up to 2.5 years. Low velocity normal impact has been induced at various time intervals before and after water immersion at energy levels of 2.5, 5 and 10 J. Following impact the plates were tested statically in compression to determine the residual strength for assessment of damage tolerance. The compression strength suffered significant reductions from the water absorption and the low velocity impact with values being dependent to the time of immersion and the water temperature. A parallel behaviour was monitored, in terms of strength reduction over time, of plates impacted prior to water immersion with the plates that contain no damage. For specimens where impact damage introduced after water immersion lower compression-after-impact (CAI) strength was observed at the same energy levels. An increase in damage diameter was evident, regardless the reinforcement type, though the gradually produced greater density of through thickness damage was responsible for the significant lower compression strength values. The presence of 0° fibres for the NCF composites as the main load bearing element dictated the sensitivity to impact as well as the corresponding residual strength. For composites with woven reinforcement, damage was contained and localized by the fabric weave and effective stress redistribution seemed to be the mechanism for the relatively higher residual strengths obtained. A semi-empirical model has been used with high accuracy in fitting the given experimental data and draw conclusions from the comparisons.

K. Berketis (✉)
Spectrum Labs SA, Efplias 49, Piraeus, Greece
e-mail: k.berketis@spectrum-labs.gr

D. Tzetzis
Department of Materials, Queen Mary College,
University of London, London E1 4NS, UK
e-mail: t.dimitris@qmul.ac.uk

Introduction

Fibre reinforced polymer composites are widely used for structural component formation such as storage tanks, ships, pipelines as well as numerous other applications primarily due to their excellent specific mechanical properties and corrosion resistance. The most important drawback is their susceptibility to damage during their service life caused by different types of impact. If the damage is easily traceable then repair procedures are followed to potentially solve the impact damage problem [1]. However, if the type of impact is of low-energy then this is considered in long term the most precarious [2, 3], since the damage can not be traced easily and subsequently repaired during routine visual inspection of the impacted surface. Specifically, delamination is notably the most serious problem, given the difficulty of its visual detection and the extent to which it lowers the mechanical properties [4]. The delamination that is generated due to the relatively low interlaminar shear strength of the composite, grow under subsequent loading and lead to a significant reduction in post-impact load-carrying capabilities. It is important in the design phase of composite structures to have data that lead to better understanding of the damage tolerance capabilities of these materials.

Damage tolerance in laminates is usually studied by determining the effect of different impact energies on their residual strength. Given that the greatest reduction after impact loading is in compression due to laminate buckling

in the delaminated areas, the compression-after-impact (CAI) test has been proposed in order to quantify the compressive reduction strength [5–8]. Numerous authors have studied the reduction of the compression residual strength on quasi-isotropic laminates, tape lay-ups and woven laminates [2, 9–18]. Nevertheless, comprehensive experimental examinations of CAI tests of GFRP composites utilising woven and non-crimp fabrics (NCF) that have been exposed to water for very long periods have not been extensively performed. One reason could be the high costs involved making such tests impractical. Though, acceleration degradation factors for long-term water immersion studies can be utilised instead [19].

Fibre reinforced polymers have excellent corrosion resistance, however, for long-term use in aqueous environments water uptake leading to weight changes is usually observed [20]. Significant debonding often appears at the interphase, and it greatly affects the weight-change kinetics and the reduction of mechanical properties [21–23]. In the case of impacted laminates there is a synergistic effect of water uptake and delamination damage that leads to gross reduction in the mechanical properties due to failure phenomena that are quite complicated in nature.

The response of GFRP composites in a deteriorated condition from water immersion to an out-of-plane impact and the associated compressive residual strength is the subject of this paper. In particular, the current investigation focuses on the behaviour of composites reinforced with plain woven and NCF that are immersed in water for periods of up to 2.5 years (30 months). The composite laminates are immersed in water at 43, 65 and 93 °C in order to accelerate the degradation mechanism. The performance of the laminates is studied through low energy impact damage while the damage tolerance is expressed by post-impact residual compressive strength.

Experimental details

Materials

The vacuum assisted resin transfer moulding technique has been used to manufacture the laminates. The resin used for impregnation was the Crystic 489 PA, produced by Scott Bader. This resin is a pre-accelerated thixotropic isophthalic polyester. The resin cures at room temperature, when 1 to 2% Catalyst M is added.

The laminates, referred to as A, B and D throughout the text, were fabricated using three different fibre reinforcement lay-ups. The naming system is described in Table 1. The first type of specimens referred to as A hitherto has a six ply $(0°, 90°)_6$ lay-up of plain woven glass fabric Chomarat 600T, by Saint Gobain. The zero direction of the fabric was set to coincide with the loading direction in compression. The second and the third materials referred to as B and D use non-crimp glass mat reinforcements produced by BTI. The B type has a lay-up of six layers of Cotech EBX-602 $(\pm 45°)_6$. The compression loading direction was at 45° to the fabric directions. The D type has a mixed lay-up of biaxial EBX-602 and triaxial ETLX-1169 fabrics laid-up as $((\pm 45°, 0°), (\pm 45°)_2, (0°, \pm 45°))$. The zero direction of the fabric was set to coincide with the loading direction in compression.

Table 1 The material types used according to the fabric architecture reinforcement and the names used to refer to them throughout the text

Material name	Fabric type	Lay-up
A	Chomarat 600T	$(0°, 90°)_6$
B	Cotech EBX-602	$(\pm 45°)_6$
D	Cotech EBX-602 Cotech ETLX-1169	$((\pm 45°, 0°), (\pm 45°)_2, (0°, \pm 45°))$

Following resin infiltration the plates were post-cured for 3 h at 80 °C. The glass fibre volume fraction was measured by the resin burn-off technique according to ASTM D2583. The volume fraction of the manufactured panels was found to be 49.7% for material type A, 42.07% for material type B and 38.52% for material type D and the average thickness of the plates was measured as 3.8 mm. Specimens with dimensions of 89 × 55 mm were cut from the panels using a diamond-tipped circular saw.

Impact tests

The free falling dart instrument used is a CEAST made Dartvis 6790. The data acquisition unit DAS4000 has capability of 1 MHz data sampling rate. Specimen plates were pneumatically clamped with a pressure of 7 bars, from top and bottom between a pair of steel plates. These plates had a 40-mm diameter window on their centres and the steel striker was of hemispherical shape with a 10-mm radius.

The striker load-cell range is 24 kN. The height was adjusted using a chain driven mechanism at 0.320 ± 0.005 m. The drop height and therefore the terminal velocity were kept constant at 2.83 m/s. The striker weight along with its launch sledge is 0.780 kg. The different levels of potential energy were achieved by increasing the weight of the striker. Using combinations of standard weights available, three impact energy levels at 2.5, 5 and 10 J were used throughout the study and four specimens were impacted at each level. The minimum impact energy level was selected so that the force registered would be above the Delamination Threshold Load [24]. This was expected to be a cause of subsequent reduction in the

in-plane mechanical properties and more specifically in compression.

Water immersion of specimens

Specimens were rested on stainless steel racks and they were immersed in deionised water, in thermostatically controlled stainless steel lined baths manufactured by Grant. The temperature controller was capable of ±0.1 °C. To accelerate the degradation process the temperatures selected were 43, 65 and 93 °C.

Compression tests

Various methods for CAI test rigs have been developed in the past with the main difference being the anti-buckling support strategy [25]. However, the rigs used in various investigations often produced compression–shear failure in the free area between the supported and the clamped zones, near the top loading plate while crushing brooming failure has been observed as well [26–29]. An evolution of the CAI rig found in Ref. [30] was designed and used for this work. The CAI test set-up is described elsewhere [23]. The specimens were loaded at 2 mm/min and the tests were terminated with the first major failure, coincident with a significant drop in the load-carrying capacity of the specimens. All the tests were conducted at room temperature conditions.

Specimen naming system

Due to the large experimental part of this work where many specimens and repetitions of specific tests were performed a solid naming system for the specimens was needed. The general nomenclature used for this paper for material marking is shown in Tables 2 and 3. For example, according to the naming system in Table 2, DIIM24 would be specimen type D impacted prior to water immersion with 5 J and then left in medium temperature, at 65 °C for 24 months to age. Also, a specimen appearing with II-IDM30, according to the naming system in Table 3 would be specimen type D left for 30 months in medium temperature of 65 °C and then impacted with 10 J.

Table 2 The specimen naming system for material impacted before water immersion

Material type	Impact level	Temperature of immersion	Length of immersion in months
A	I = 2.5 J	L = 43 °C	1–30
B	II = 5 J	M = 65 °C	
D	III = 10 J	H = 93 °C	
X	YYY	Z	W

If there is no impact, YYY is omitted

Table 3 The specimen naming system for material impacted after water immersion

Impact level	Material type	Temperature of immersion	Length of immersion in months
I = 2.5 J	A	L = 43 °C	1–30
II = 5 J	B	M = 65 °C	
III = 10 J	D	H = 93 °C	
YYY	X	Z	W

If there is no impact, YYY is omitted

Results and discussion

Reference specimens

A series of tests were performed on specimens with no environmental exposure to obtain the dry reference material properties. Only the result of impact damage on residual compressive strength is considered. The effects of the different fibre reinforcement architecture and placement on residual compressive strength after impact are presented in Fig. 1 for material types A, B and D, respectively. Some initial lag at the start of some of the graphs is related to the testing procedures followed. For specimens of type A and D, where fibres are present in the 0° direction, both strength and stiffness are relatively higher than that of specimens of material type B which have no fibres along the 0° direction. Evidently, from the graphs presented the apparent plate stiffness, for all material types individually, does not change considerably with increasing damage size, within the range of impact energies studied. From Fig. 1b it can be seen that material type B experiences extensive non-linear deformation. This behaviour is seen due to the ±45° reinforcement. This material allows for extensive in-plane shear. Due to the lack of 0° fibre reinforcement, local microbuckling is possible without extensive fibre breakage. This type of behaviour leads to extensive lateral deformation.

A comparison of the results obtained from the CAI strength of the reference specimens of all 3 types of materials available is presented in Figs. 2 and 3. The values of compressive strength in Table 4 represent the average value of 4 specimens per material type. Over the range of impact energies tested as shown in Fig. 2, for materials A and D a significant drop in compressive strength is observed. For the material B the initial strength was low due to the reinforcement orientation. The effect of impact damage on the residual compressive strength is less marked in material type B. This is mainly due to the non-existence

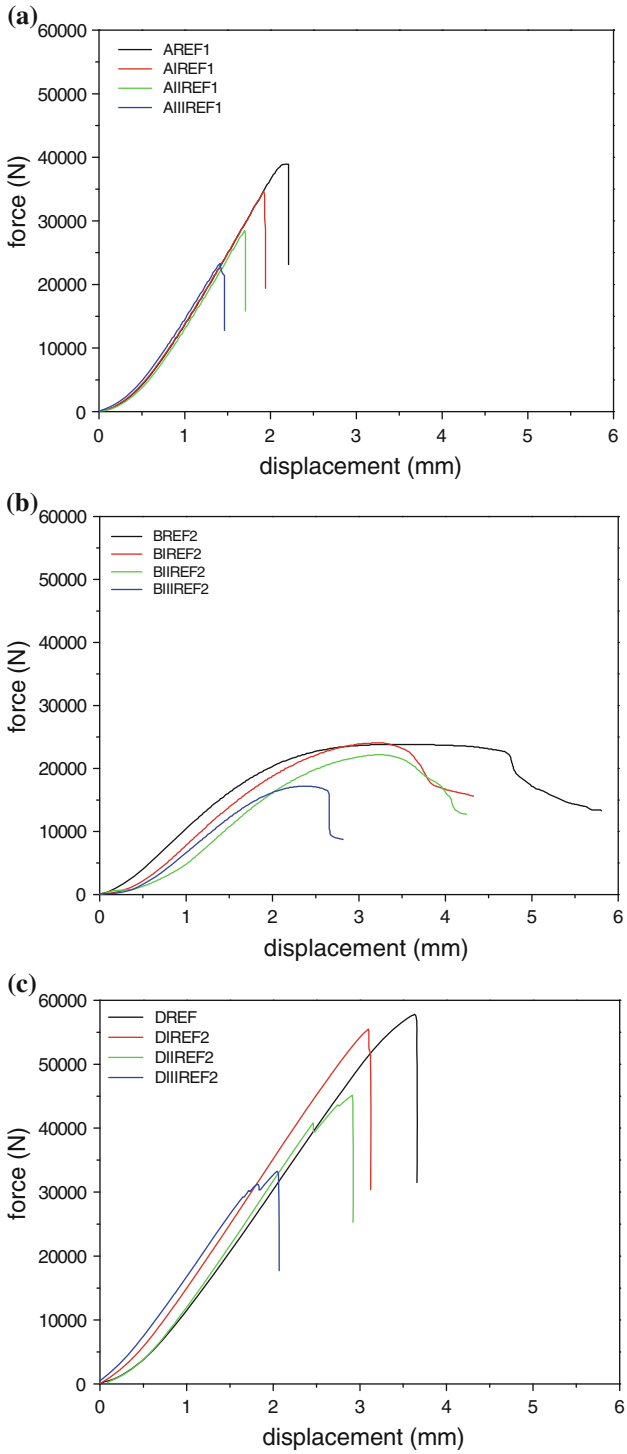

Fig. 1 Force–displacement diagrams for the dry reference materials types A, B and D. *Roman numerals* I, II and III are for impact levels 2.5, 5 and 10 J, respectively

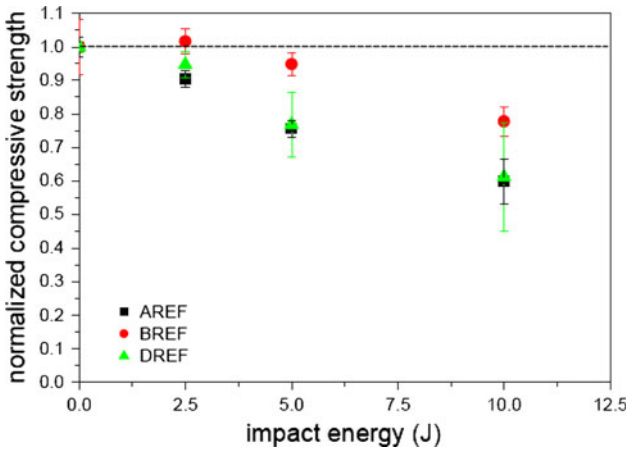

Fig. 2 Normalized compressive strength with respect to impact energy for the reference materials

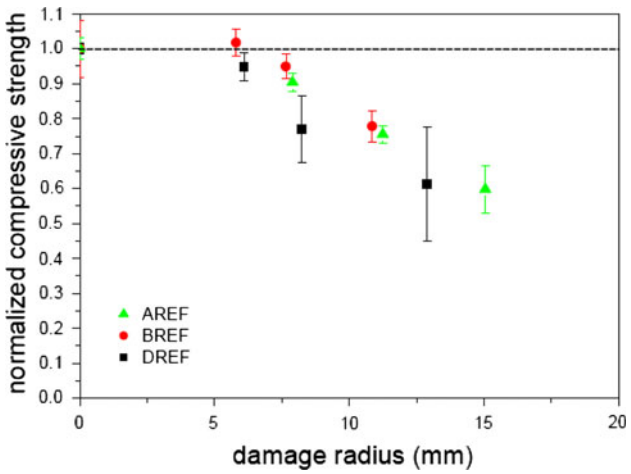

Fig. 3 Normalized compressive strength against horizontal damage radius for dry reference materials

Table 4 Compressive strength of dry undamaged reference specimens A, B and D

Material type	Compressive strength	St. Dev.
A	229.23	6.98
B	117.37	9.67
D	268.81	4.42

of 0° fibres, which when their loading bearing capacity is reduced by damage, there follows a large drop in compressive strength as is the case of materials A and D. In fact at 2.5 J impact, slightly higher strength is observed for material type B when compared to undamaged plate strength. It can be assumed that the damage in the centre of the specimens caused by impact creates a ply interlocking effect that reduces the excessive deformation allowed otherwise by this fibre architecture and placement combination. This in turn allows for the slightly higher compressive strength retention compared to undamaged specimens.

In Fig. 3, the normalized compressive strength retention of material type B is the highest, when compared to

material type A but mainly to material type D for any given damage size. Compared to material type D, at similar level of normalized strength retention at ~75% the original undamaged, the damage radius for material type D is about 7 mm whereas for material types B and A is about 11 mm. As material type B has no fibres in the 0° direction, strength retention is not significantly affected by increasing damage size. During impact, increased bending and larger damage areas overall were observed. The result can be seen on Fig. 3 as for the fourth point, at 10 J impact, significantly larger radius compared to rest of the materials is seen.

The increased damage tolerance of material type A is due to the woven reinforcement used. The initial undamaged strength using this type of reinforcement is lower than what can be obtained using NCF. This is because the crimping of the tows causes local friction and premature breaking of the fibres. CAI and the compression loading mode in general is about stability and effective stress redistribution. The residual compressive strength loss is more abrupt for impacted NCF reinforced composites because after damage of the 0° fibres there is no effective way for stress redistribution. In the case of material type D this is evident in Fig. 3 by the sharper slope of the normalized compressive strength with respect to damage radius. Material type A is capable to redistribute the compressive stresses around the impact damaged areas better and so it can sustain much larger damage whilst taking comparable load to material type D.

Water conditioned material

The water exposure causes a significant strength reduction at the high temperature of 93 °C. At the medium temperature of 65 °C, strength reduction is more gradual. At the low temperature of 43 °C, still there is a strength reduction of the plates, although to a much lesser extent than that caused by the higher temperature exposure. Strength reduction at the low temperature is evident even if no impact damage is present. Typical force–deformation curves obtained at all three test temperatures are presented in Figs. 4, 5 and 6 for material type A, B and D, respectively. It becomes evident that even low temperature water immersion causes a significant drop in the residual compressive strength, even if no impact damage is present. The rate of this strength reduction is time and temperature dependant with temperature of immersion being more important. It is seen that the levels of strength reduction attained after water immersion at 93 °C for 3 months are nearly met after 30 months of immersion at 65 °C for material type A. For material types B and D the level of strength retention is higher at 65 °C after 30 months of immersion compared to the 3 months at 93 °C. From

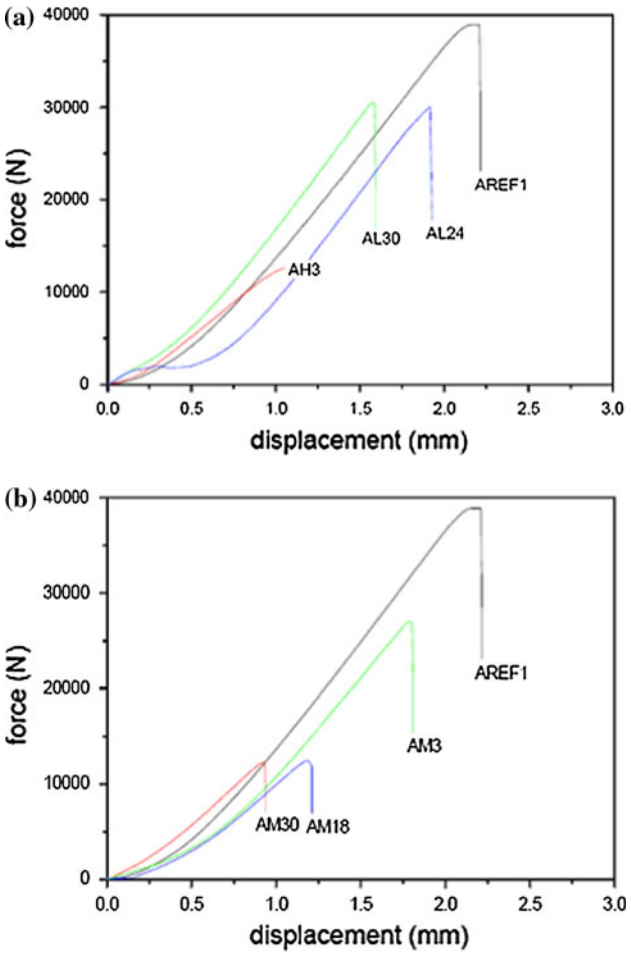

Fig. 4 The force–displacement curves of undamaged material type A after water immersion at 45 °C (*L*) and 93 °C (*H*) in (**a**) and 65 °C (*M*) in (**b**). *Numbers* signify the duration of immersion in water. Dry reference samples are marked *REF1*

Fig. 5, it is clear that the CAI rig used allowed for the extensive vertical and horizontal expansion that was needed for the specimens of material type B. It is significant to be noted that there is a sustained load, with no reduction for large part of these curves. The shape of these specimens after the end of the tests was barrel like.

The residual compressive strength after water immersion for all three material types A, B and D are compared in Fig. 7 for the medium temperature of 65 °C and for the low temperature of 43 °C. From the results presented in Fig. 7b it can be seen that an overall a reduction ranging between ~8% for material type D to a maximum of ~23% for material type A is caused after 30 months of water immersion at 43 °C. At 65 °C the compressive strength reduction in Fig. 7a is markedly more significant compared to that at 43 °C. For the NCF reinforced materials the reduction is ~58% the initial undamaged strength, whereas for the woven type A is ~66% the initial undamaged strength. The level of difference measured ascertains the effect of the

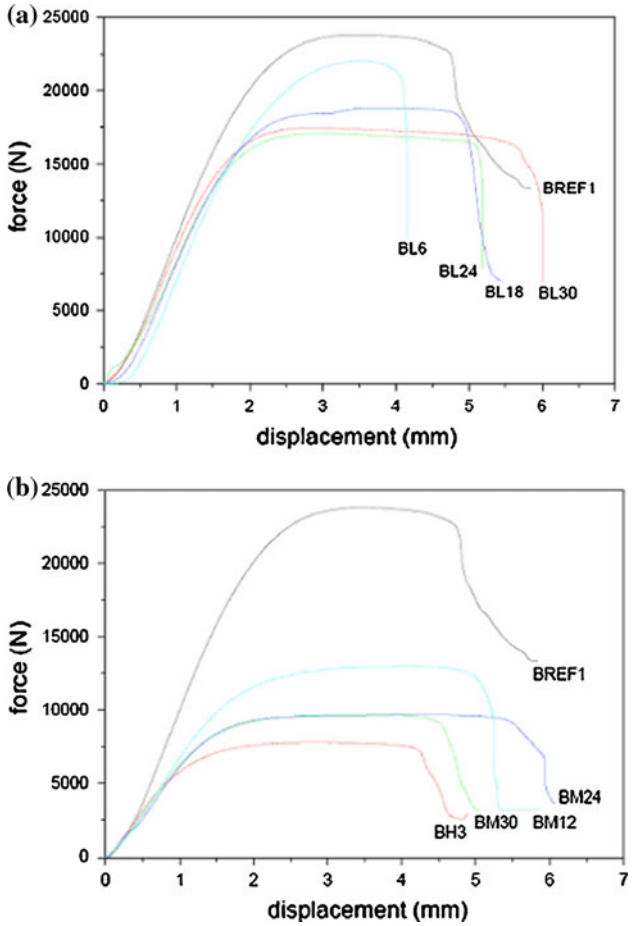

Fig. 5 The force–displacement curves of undamaged material type B after water immersion at 45 °C (*L*) in (**a**) and 93 °C (*H*) and 65 °C (*M*) in (**b**). *Numbers* signify the duration of immersion in water. Dry reference samples are marked *REF1*

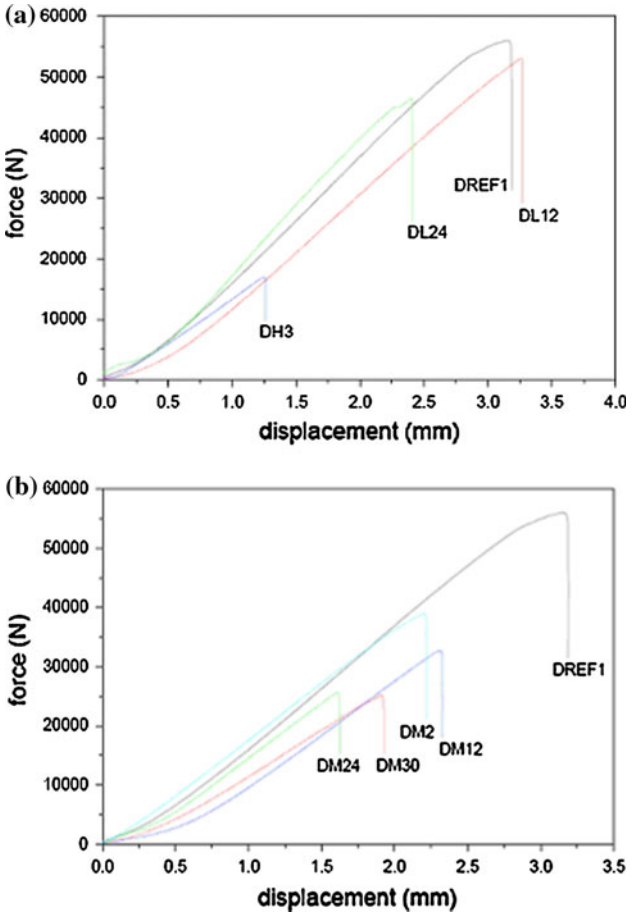

Fig. 6 The force–displacement curves of undamaged material type D after water immersion at 45 °C (*L*) and 93 °C (*H*) in (**a**) and 65 °C (*M*) in (**b**). *Numbers* signify the duration of immersion in water. Dry reference samples are marked *REF1*

fabric reinforcement in the residual strength retention after long-term water immersion.

Strength comparison for specimens impacted prior and after water immersion

The differences in residual compressive strength for specimens exposed to water already containing impact damage with the specimens impacted at the same energy after water exposure are presented in this section. In Figs. 8, 9 and 10 the change of residual compressive strength with respect to time of water immersion is presented for material type A, B and D, respectively. The general trend is that the residual compressive strength when the impact takes place after environmental exposure is lower compared to specimens exposed to water already containing some damage. The significant drop in residual compressive strength after exposure at 93 °C for 3 months is also evident. The compressive strength drops well below the 30% of the original "equivalent" strength [31], which points out the synergistic effect of degradation due to water exposure and impact damage.

In Fig. 11 the normalized compressive strength with respect to time of immersion in water at 65 °C, for material type D, for impact before and after immersion is plotted. Normalization of compressive strength is performed against the undamaged compressive strength of specimens after the given immersion time. An important finding is the parallel behaviour, in terms of strength reduction over time, of plates impacted prior to water immersion with the plates that contain no damage. A clustering of the REF marked material with that that contains damage from the start of the experiments is clearly shown in Fig. 11. Another relevant finding is the clustering of the curves for specimens impacted after water immersion. The actual impact energy with which they have been stroked seems to become not important. The impact energy level does not significantly differentiate the slopes or the level of the curves obtained.

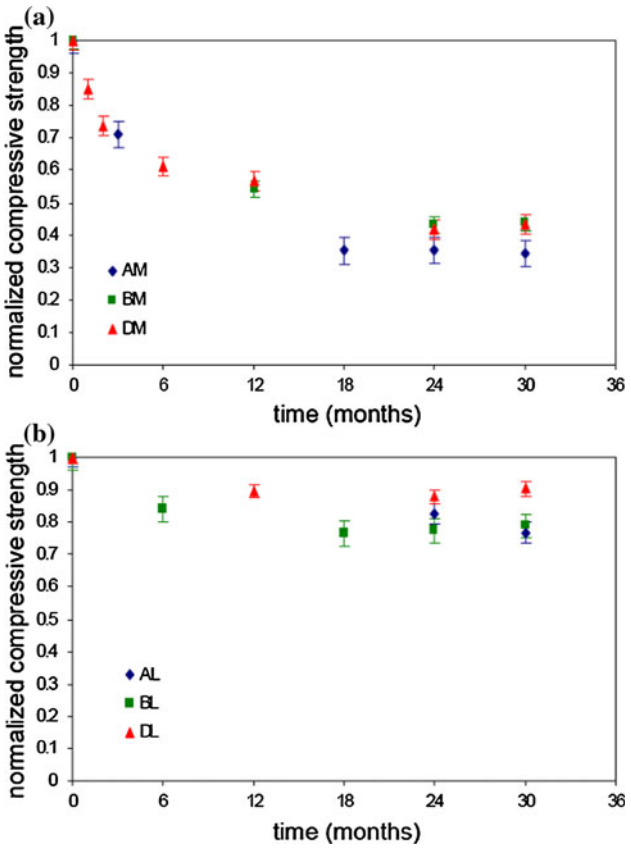

Fig. 7 The normalized compressive strength after water immersion of all three specimen types A, B and D at **a** the medium temperature M of 65 °C and **b** the low temperature L of 43 °C

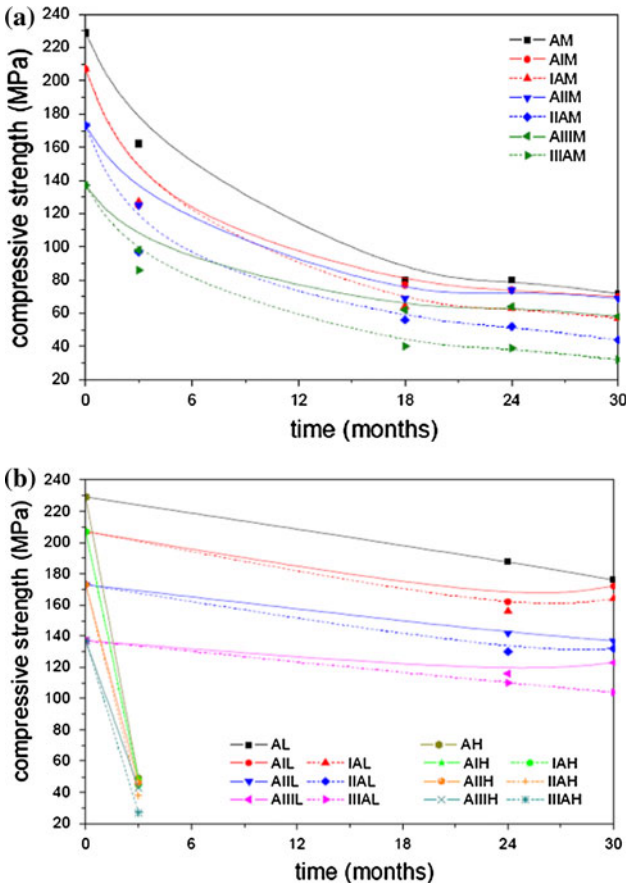

Fig. 8 The residual compressive strength after impact and exposure to water at medium *M* (65 °C) in (**a**) and low *L* (43 °C) and high *H* (93 °C) in (**b**) temperature is presented for material type A with respect to time. *Dotted lines* signify specimens impacted after water exposure. Specimens marked with *I*, *II* and *III* are impacted with 2.5, 5 and 10 J, respectively. The *roman numerals* precede for impact after water immersion

Effects of damage size on residual compressive strength

The effect of damage size, caused by increasing the impact energy, combined with the effects of water immersion on the residual compressive strength of specimens is investigated in this section. Using an air-coupled ultrasonic C-Scan system available [32] the damage size caused by impact was measured. From the results presented the lower strength of specimens impacted after water immersion, compared to pre-impacted specimens, is expected to be related to the increasing severity of the damage with respect to time of immersion. Strength reduction has traditionally been related to horizontal damage width. A general increase in damage diameter for specimens impacted at the same impact levels of 2.5, 5 and 10 J after water immersion is evident in Fig. 12. This is not always true though as can be seen for the 2-month long exposed at 65 °C. Matrix softening effects could act that allowed for smaller damage size. The contribution of the reduced damage size at that time is a less pronounced strength reduction.

Had it been damage size only related the difference between pre and post-immersion impact, data points should have been on common curves for a given time line in Fig. 13. This is not the case based on the results presented in this paper due to the fact that damage inflicted on wet composites can not be characterized merely by 2D means [23]. Although the damage size caused by impact after immersion is increased compared to the size of damage caused by same impact energy before water immersion, the intensity of damage needs to be addressed. Post-impact, a qualitative measure of this impact damage intensity can be obtained by studying and comparing data obtained by the drop weight impact testing machine; in particular, damage intensity can be linked to the maximum force registered and the difference in absorbed energy before and after water immersion [33].

Compression fracture patterns

Depending on the type and architecture of reinforcement different fracture patterns were observed. Due to the design

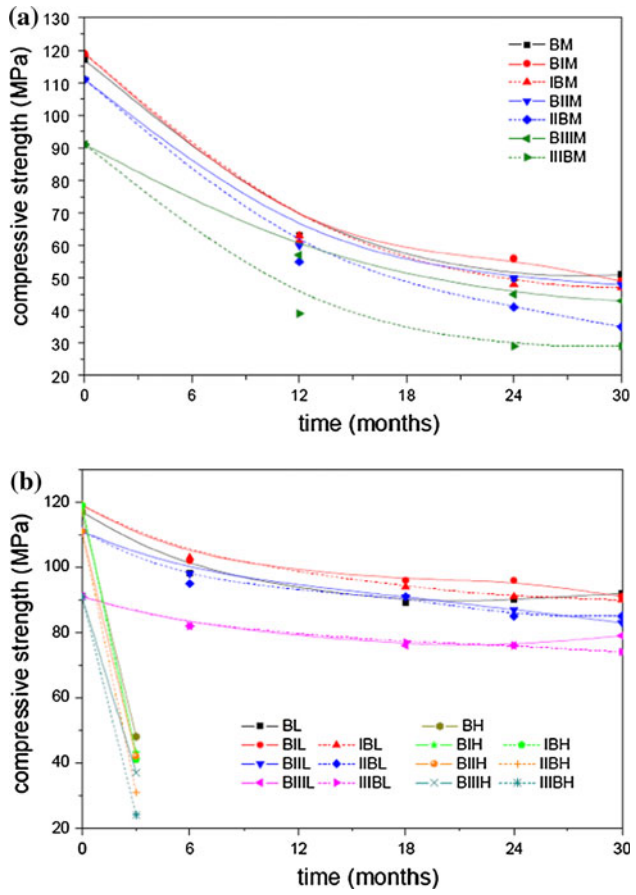

Fig. 9 The residual compressive strength after impact and exposure to water at medium *M* (65 °C) in (**a**) and low *L* (43 °C) and high *H* (93 °C) in (**b**) temperature is presented for material type B with respect to time. *Dotted lines* signify specimens impacted after water exposure. Specimens marked with *I*, *II* and *III* are impacted with 2.5, 5 and 10 J, respectively. The roman numerals precede for impact after water immersion

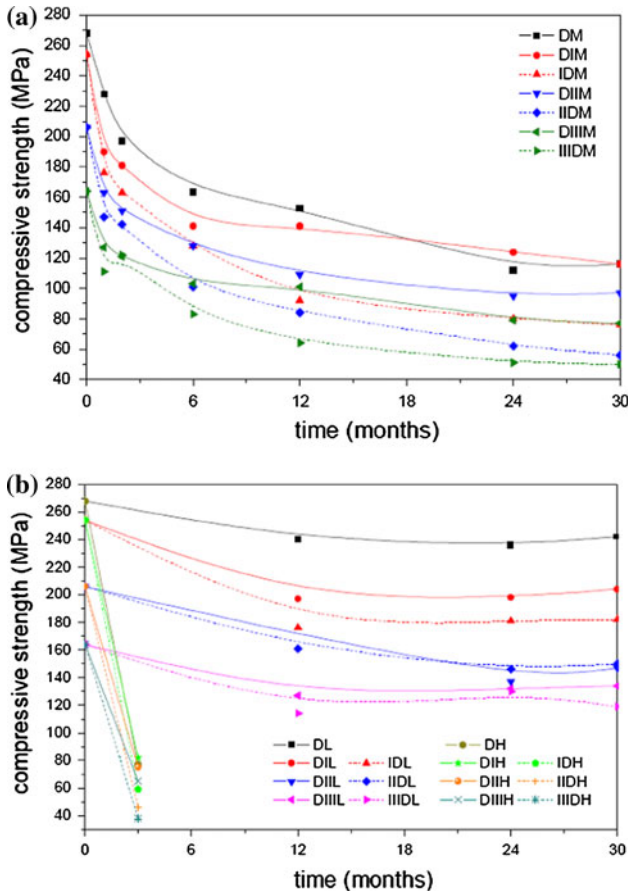

Fig. 10 The residual compressive strength after impact and exposure to water at medium *M* (65 °C) in (**a**) and low *L* (43 °C) and high *H* (93 °C) in (**b**) temperature is presented for material type D with respect to time. *Dotted lines* signify specimens impacted after water exposure. Specimens marked with *I*, *II* and *III* are impacted with 2.5, 5 and 10 J, respectively. The roman numerals precede for impact after water immersion

of the test fixture used for the CAI tests, the boundary conditions set restrained global buckling from being the mode of failure. Thus, mainly two modes of failure were observed. For the woven type A and the triaxial type D specimens failure was linked with microbuckling of the 0° fibres. Given the boundary conditions imposed by the test fixture, the failure mode did not change regardless of the impact energy, the immersion duration or whether impact predated or not immersion as in Figs. 14 and 15.

For specimens type B with the biaxial ±45° fabric reinforcement the failure mode observed was distinctively different. Given the lack of 0° reinforcement, failure direction followed the orientation of the reinforcement fabric as shown in Fig. 16. Although the damage sustained by type B specimens after water immersion was visibly more serious, with partial penetration being the normal at 65 °C, overall they prove to be more damage tolerant compared to specimens type A and D. Taking for example the situation where impact at 10 J, takes place after an immersion of 30 months at 65 °C, reduction of residual strength for type B specimens is to 30% the initial whereas for type A is 21% and for type D is 18%. This can mainly be attributed to the fact that the great strength reduction in material types A and D is associated with the 0° reinforcement. When these get damaged severe strength loss is imparted. In the case of material type B, the initial strength is low due to the lack of 0° fibre reinforcement so the ratio between reduced and original strength is larger.

Water immersion has in the long-term, negative effect on compressive strength. This strength reduction can be attributed to both physical and chemical changes. Physical hygrothermal changes experienced by the materials under study included the appearance of internal stresses caused by diffusing water, whose manifestation took the form of matrix cracking and matrix plasticization [20]. Chemical changes can take the form of hydrolysis of the polyester

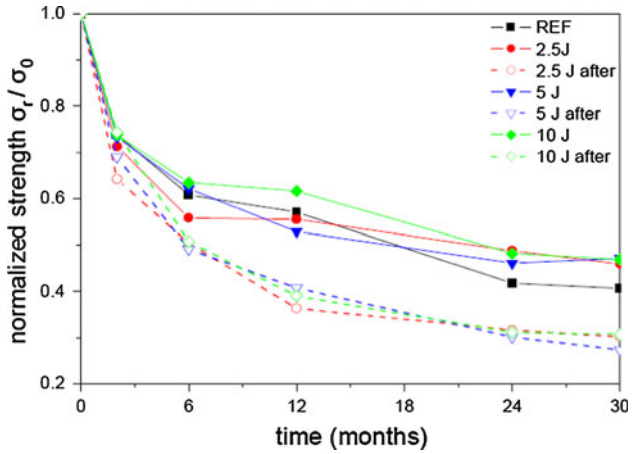

Fig. 11 Normalized residual compressive strength over time for material type D at 65 °C. Specimens marked after have been impacted after water immersion. Normalization for each set of specimens tested from different water immersion period is performed against the residual compressive strength of undamaged material after the given immersion time

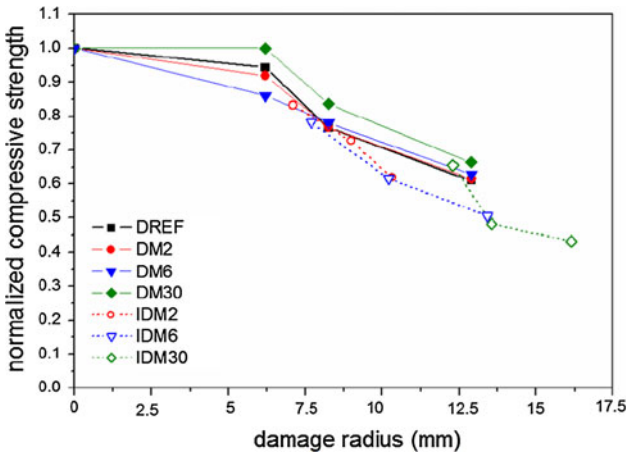

Fig. 13 Normalized compressive strength over damage radius. Normalization is performed against undamaged strength at the given immersion duration. Duration is specified by the numbers on the specimen names, all materials type D, immersion at 65 °C

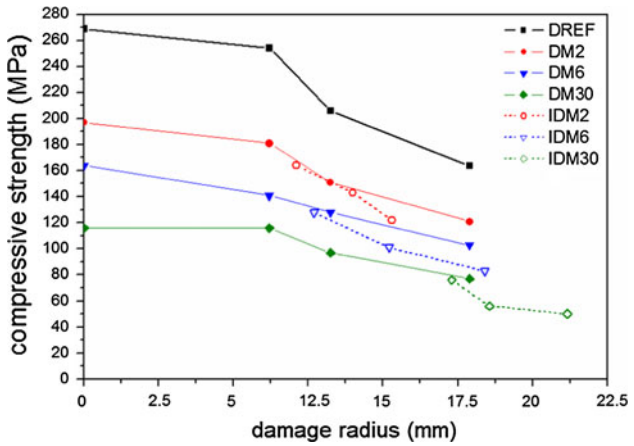

Fig. 12 Compressive strength over damage radius. The damage of specimens impacted before water immersion is assumed to be constant overtime. Specimens marked with *I* on the legend refer to cases impacted after water immersion for a length of time in months, equal to the number given. All specimens are of type D immersed at 65 °C, except for the references marked *REF* which have not been in water

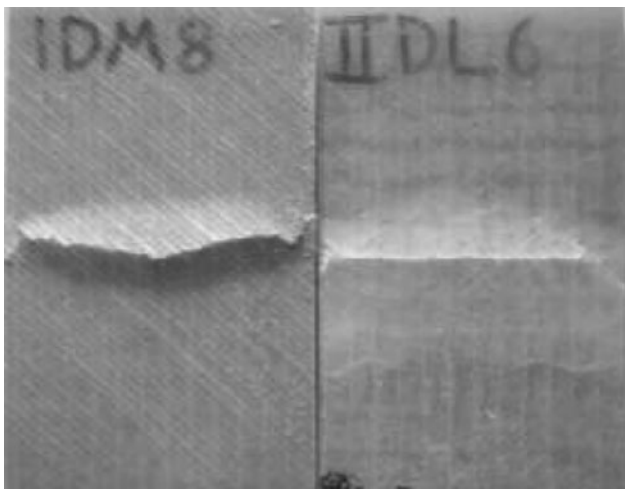

Fig. 14 Failure mode of specimens type D in CAI. The specimen on the *left* marked IDM8 has been impacted after immersion in water at 65 °C with 2.5 J. The specimen on the *right* marked IIDL6 has been impacted after water immersion in water at 43 °C at 5 J. Duration of immersion for both specimens was 24 months

network, attack on the fibre-matrix interface and attack on the glass fibres [34, 35] which all contributed to the strength loss encountered, although the role of each individual mechanism was not specifically studied in the current context.

Strength prediction model

A semi-empirical model by Caprino [36] based on linear elastic fracture mechanics LEFM concepts is proposed for the prediction of residual compressive strength after impact. The main idea of this model is that of equalizing the impact area with a hole or a reduced stiffness elastic inclusion. The model assumes that there is a characteristic defect dimension, which needs to be found experimentally. Its form as used here is:

$$\frac{\sigma_r}{\sigma_0} = \left(\frac{R_0}{R}\right)^m \tag{1}$$

where σ_r represents the residual strength of the notched laminate, σ_0 is the initial undamaged strength, R is the dimension of the notch, m is an experimentally obtained parameter.

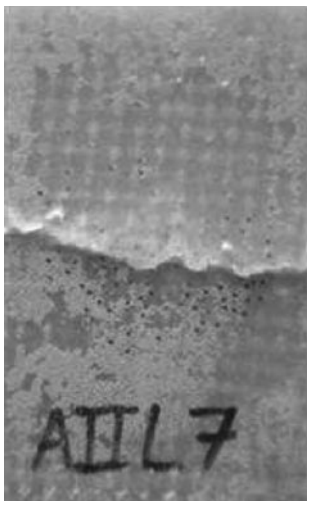

Fig. 15 Specimen type A impacted before immersion with 5 J immersed in water for 24 months at 43 °C

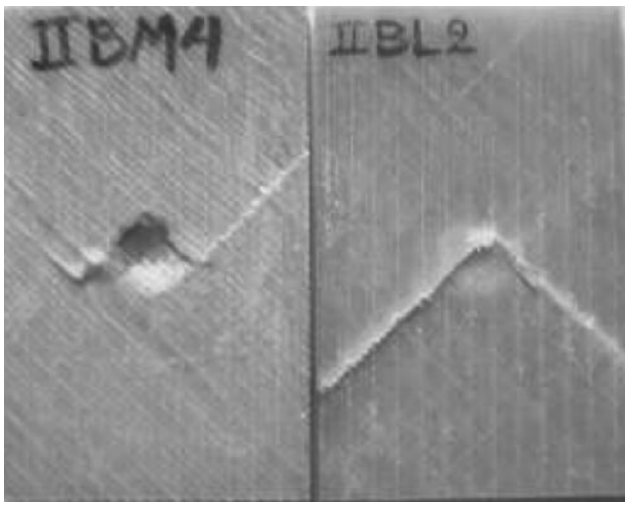

Fig. 16 Specimens type B impacted with 5 J after 30 months water immersion. The specimen on the *left* marked IIBM4 has been in water at 65 °C and the specimen on the right at 43 °C

When $R \leq R_0$ no strength reduction is associated with the composite. The model, although it is not environmental degradation specific, the parameter R_0 if corrected for the effects of environmental exposure could be used for correlation.

Increased sensitivity in fitting points is allowed due to the two variable parameters formulation of the model. This can be seen in Fig. 17 where the normalized residual compressive strength after impact of dry reference specimens against impact damage radius is plotted. It can be deduced that Caprino's model can be used with high accuracy in fitting the given experimental data. Material type D is seen here again to be the most sensitive to impact. Both material types A and B are more resistant compared

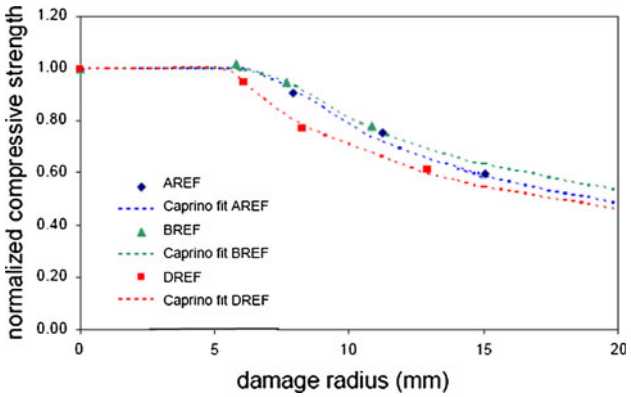

Fig. 17 Comparison of the normalized post-impact residual compressive strength of the three dry impacted reference materials A, B and D with respect to damage radius measured. *Dashed lines* are the best fit of Caprino's model

to material D but for different reasons. The biaxial ±45° B type material seems not so sensitive to impact and the corresponding residual strength does not reduce sharply because of lack of 0° fibres that are the main load bearing elements. On the other hand in material type A which has woven reinforcement, damage is contained and localized by the fabric weave and effective stress redistribution can take place which helps keeping relatively high residual strength.

In Fig. 17 the compressive residual strength after 2.5 J impact for material type B is higher than the initial undamaged compressive strength. The mathematical formulation of Caprino's model does not allow for a solution above 1 though. A similar situation with different material has been reported elsewhere [37]. This case can be explained if a small damage as such acts in a way as to lock layers not allowing them to move in-plane shear.

Further on, the model is tested for fit on material with impact damage existing and induced after water immersion. Specifically, due to the highly non-linear behaviour exhibited by material type B in compression after water immersion, it was decided not to pursue further with fitting the residual strength model. Representative fitting curves for CAI results of material type A and D are shown in Figs. 18 and 19, respectively. From the results it can be seen that the model for prediction of residual compressive strength has the ability to fit data points well. The restriction faced with this model is that there was found no apparent trend in the curve fitting parameters R_0 and m. Residual compressive strength, especially of water immersed specimens, does not depend solely on a 2D damage size measured mainly as the extent of delaminations. Through the thickness damage, mainly in the form of broken fibres, becomes increasingly more important when the matrix has degraded after prolonged water immersion

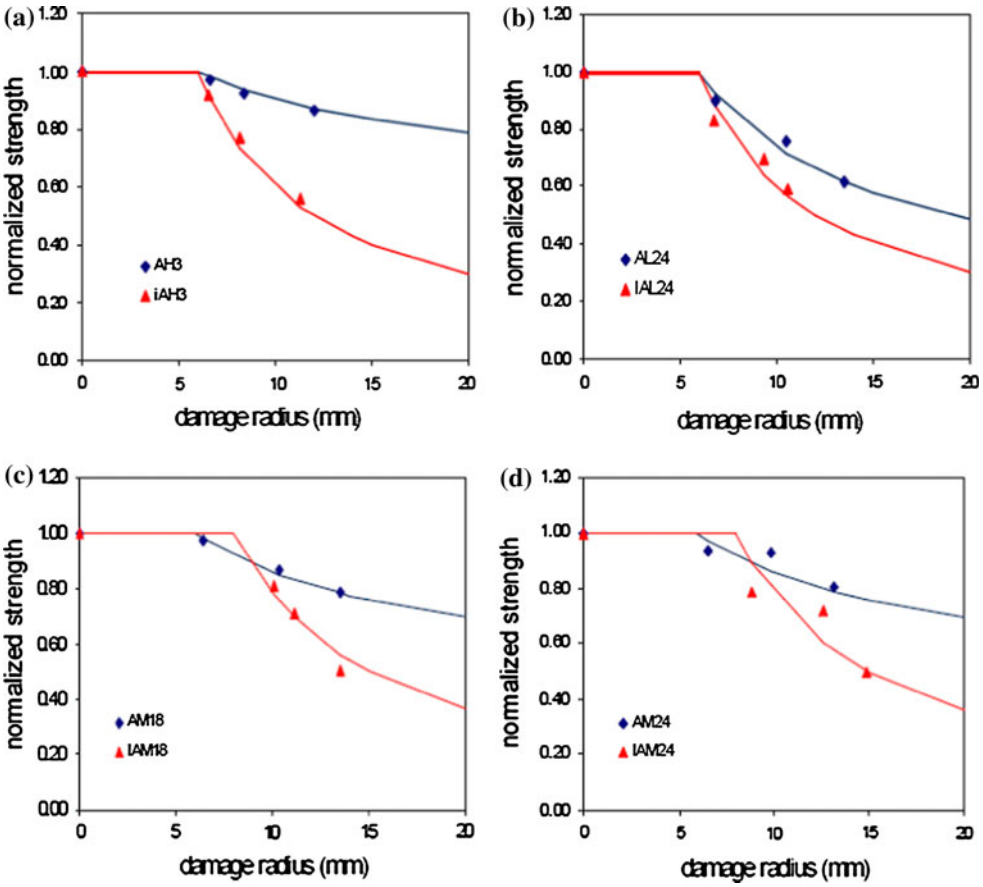

Fig. 18 Normalized compression after impact strength of specimens type A with respect to impact damage radius. *Lines* fit represent Caprino's model. *H*, *M* and *L* signify exposure temperature of 93, 65 and 43 °C, respectively. The duration of immersion is the number next to the specimen name in months. Specimens impacted after water immersion are marked as *IA*

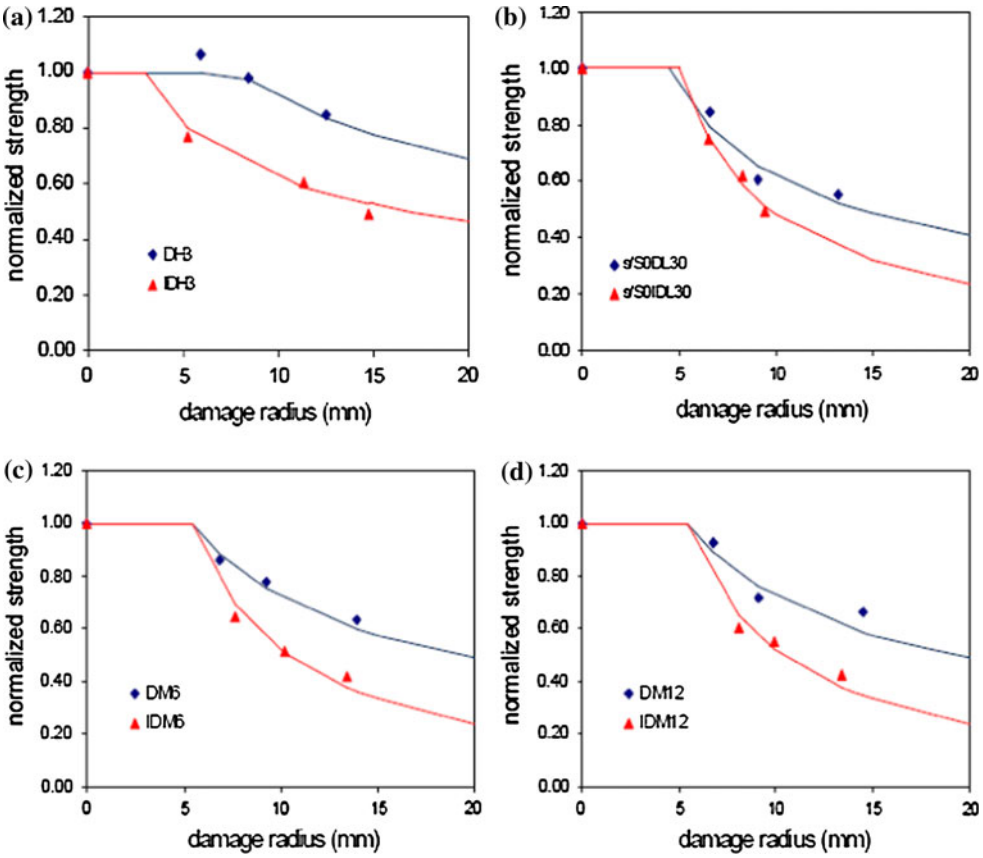

Fig. 19 Normalized compression after impact strength of specimens type D with respect to impact damage diameter. *Lines* represent best fit of Caprino's model. *M* and *L* signify exposure temperature of 65 and 43 °C, respectively. The duration of immersion is the number next to the specimen name in months. Specimens impacted after immersion are marked as *IA*

and the model formulation does not allow for adjustments in this respect.

Conclusion

Low velocity impact, at the levels of energy studied, was seen to cause compressive strength reduction. Material type B showed highly no linear behaviour compared with material type D and A since it had no 0° reinforcement. Material type A was found to be more damage tolerant than type D as material type A could still sustain the same compressive load with much larger damage.

Environmental exposure causes a marked reduction on the residual compressive strength even if no impact damage is present. The highest reduction in compressive strength was obtained after immersion at 93 °C for 3 months with values between ~28 and ~40% of the original dry strength. Even after 30 months immersion at 65 °C the strength reduction was not as high as at the 93 °C, ranging between ~34 and ~48% the original dry strength. At 43° the strength loss after 30 months, was much less, in the region of ~77 to ~92% of initial dry strength.

Impact damage introduced after water immersion was shown to cause larger strength reduction when compared to impact introduced before water immersion at the same energy levels. The size of damage and the intensity associated with impact after water immersion have also been shown to increase compared to the size of damage on dry specimens at same impact energy levels. The severity of damage caused by impact increases with length of time and temperature. This is a consequence of the fact that material immersed in water degrades, this degradation being a function of time and temperature.

The results of residual compression strength compare well with predictions of a semi-empirical model of Caprino. The problem arose when trying to generalize it to pre and post-water immersion impacted specimens as the values of the parameters obtained did not show identifiable trends. It is evident that size of damage, when immersion preceded impact, does not follow a simple rule. The complex effects of the environment on the composite plates can be held responsible. It was established that water immersion changes the nature of the damage inflicted by the striker and that damage after water immersion can not be described merely in two dimensions. A damage intensity parameter linked to three-dimensional spread of the damage is needed and future work will address this point. Models using a fracture mechanics approach to strength prediction where damage is modelled as a two-dimensional crack of some form have limited applicability in the case of compressive strength prediction when impact occurs after water immersion.

References

1. Tzetzis D, Hogg PJ (2008) Mater Des 29(2):436
2. De Freitas M, Reis L (1998) Compos Struct 42(4):365
3. Xiong Y, Poon C, Straznicky PV, Vietinghoff H (1995) Compos Struct 30(4):357
4. Baker AA, Jones R, Callinan RJ (1985) Compos Struct 4(1):15
5. NASA (1983) Standard test for toughened resin composites. NASA Reference Publication 1092
6. Boeing (1988) Advanced composite compression test. Boeing Specification Support Standard BSS 7260
7. SACMA (1994) Recommended Methods SRM 2-94. Suppliers of Advanced Composites Materials Association
8. Curtis PT (1988) CRAG test methods for the measurements of the engineering properties of fibre reinforced plastics. Royal Aerospace Establishment Technical Report TR88012
9. Delfosse D, Poursartip A, Coxon BR, Dost EF (1995) Compos Mater: Fatigue Fract 5:333. ASTM STP 1230
10. Hawyes VJ, Curtis PT, Soutis C (2001) Compos Part A: Appl Sci Manuf 32(9):1263
11. Duarte A, Herszberg I, Paton R (1999) Compos Struct 47 (1–4):753
12. Dorey G, Bishop SM, Curtis PT (1985) Compos Sci Technol 23(3):221
13. Habib FA (2001) Compos Struct 53:309
14. Bishop SM (1985) Compos Struct 3:295
15. Kim J, Shioya M, Kobayashi H, Kaneko J, Kido M (2004) Compos Sci Technol 64:2221
16. Kim JK, Sham ML (2000) Compos Sci Technol 60:745
17. Bibo GA, Hogg PJ (1998) Key Eng Mater 141–143:93
18. Cantwell WJ, Morton J (1991) Composites 22(5):347
19. Bank LC, Gentry TR, Barkatt A (1995) J Reinf Plast Compos 14:559
20. Berketis K, Tzetzis D (2009) J Mater Sci 44:3578. doi: 10.1007/s10853-009-3485-9
21. Morii T, Hamada H, Maekawa Z, Tanimoto T, Hirano T, Kiyosumi K (1983) Polym Compos 1:3744
22. Morii T, Hamada H, Maekawa Z, Tanimoto T, Hirano T, Kiyosumi K (1994) Polym Compos 15:206
23. Berketis K, Tzetzis D, Hogg PJ (2008) Mater Des 29:1300
24. Shoeppner GA, Abrate S (2000) Compos Part A 31:903
25. Sanchez-Saez S, Barbero E, Zaera R, Navarro C (2005) Compos Sci Technol 65:1911
26. Nettles AT, Hodge AJ (1991) Compression-after-impact testing of thin composite materials. In: Proceedings of the 23rd international SAMPE technical conference, pp 177–183
27. Liu D, Raju BB, Dang X (1998) Int J Impact Eng 21:837
28. Sjoblom PO, Hwang B (1989) Compression-after-impact: the $5000 data point. In: International SAMPE Symposium Exhibition, vol 34, pp 1411–1421
29. Prichard JC, Hogg PJ (1990) Composites 21:503
30. Prichard JC, Hogg PJ, Stone DL (1992) A miniaturized post impact compression test. Department of Materials, Queen Mary and Westfield College in co-operation with British Aerospace and CIBA Geigy, pp 1–8
31. Zhou G (1996) Compos Struct 35:171
32. Berketis K, Tzetzis D, Hogg PJ (2009) Polym Compos 30(8):1043
33. Berketis K, Tzetzis D (2009) In: Lechkov M, Prandzheva S (eds) Encyclopedia of polymer composites. Nova Science Publishers, Inc, New York. ISBN: 978-1-60741-717-0
34. Schutte CL (1994) Mater Sci Eng R 13:265
35. Belan F, Bellenger V, Mortaigne B (1997) Polym Degrad Stab 56:93
36. Caprino G (1983) J Compos Mater 18:508

37. Komai K, Minoshima K, Yamasaki H (1995) Evaluation of low-velocity impact induced delamination by scanning acoustic microscope and influence of water absorption on delamination and compression after impact of CFRP. In: Emri I, Knauss WG (eds) First international conference on the mechanics of time dependent materials, SEM, pp 287–292